Chapter 4

Multiple Protein Secretion Profiling Analysis of Single Cells and Small Cell Colonies with Integrated Barcode Chip

4.1 Introduction

One of the major barriers in cancer research is the complexity. All cancers such as breast, prostate, lung, and brain cancer, etc., can be identified as multiple diseases with different genetic and environmental mutations. The complexity and heterogeneity of cancer require a systemic approach for diagnosis as well as treatment, aiming to find key elements responsible for the emergent properties of cancer.[1–3] Those elements include individual biomolecules such as DNAs, RNAs, and proteins with specific mutations and networks modulating a series of biological process that leads to cancerous properties such as metastatic potential, immortality, and resistance to therapies. Especially, secreted proteins are an attractive target for cancer research because they can define cell characteristics and they are active agents to interact with the environment including other cells, the so-called tumor microenvironment. Cancer cells can induce adjacent stroma cells and extracellular matrix (ECM) to form a supportive microenvironment by producing stroma-modulating growth factors.[4] Immune cells such as macrophages and neutrophils can also contribute to tumor progression by expressing proteases or pro-angiogenic factors. Thus, monitoring secreted proteins in a multiplexed manner from individual cells is a useful tool for the basic

research as well as the clinical diagnosis and treatment. Heterogeneity of tumor microenvironment also requires comprehensive characterization of functional phenotypes at the single cell level.

Representative techniques for single-cell functional assay are fluorescence-activated cell sorting (FACS)[5] and ELISpot,[6] a variant of the Enzyme-Linked Immunosorbent Assay (ELISA). FACS is commonly utilized to detect and sort cells via their surface markers. However, by blocking vesicle transport followed by staining of proteins in the cytoplasm, FACS can extend its use for the detection of protein secretion. An ELISpot test can indicate the footprint of single-cell secretion by capturing secreted proteins located proximal to the cells. Both of the techniques are currently used in clinical application but sensitivity, limited multiplexing capability, high cost, and the requirement of a large amount of sample limits their widespread use. Therefore, a new platform for the multiplexed protein detection is needed which is simple, fast, and easily expandable, at low cost.

Here, we report on an integrated barcode chip that enables high-content assessment of glioblastoma (GBM) brain tumor cells. GBM is the most common malignant brain tumor in adults, and is the most lethal of all cancers. As the name of the tumor indicates, GBM has extensive genetic and biological variability, heterogeneous clinical behavior, and accordingly unpredictable, poor prognostics[7]. Thus, studying GBM requires dealing with the heterogeneous and complex characteristics, which is a good target for our platform equipped with the capability of multiplexing analysis. The integrated barcode chip is comprised of 360 microchambers in which an antibody barcode array for the measurement of a dozen proteins is patterned. In this study, we measured protein secretion profiles from four GBM cell lines, each with specific mutation, and observed profound cellular

heterogeneity, along with unique features only available at the single-cell level. We found anti-correlations between two proteins, MIF and VEGF, which couldn't be identified with conventional, bulk analysis. We also confirmed the tumor-suppressing activity of PTEN in GBM cell lines by comparing the protein secretion profiles of two cell lines, one with PTEN and the other without PTEN. The optical transparency of our platform enabled us to monitor the physical characteristics of the system, which were matched up with the secretion profile later and presented the cell–cell communication effect through epithermal growth factor receptor (EGFR). We further demonstrate that this platform can be extended to the analysis of solid tumors by measuring secreted proteins from single cells and small cell colonies derived from the tumor of a patient. Even though there is heterogeneity in cellular functions, as we confirmed with our platform, we can also attain statistically meaningful analysis owing to the large amount of data sets that we can obtain from a single experiment.

4.2 Experimental Methods

4.2.1 Patterning of DNA barcode arrays

The DNA barcode array was prepared by microfluidic flow patterning and the microfludic-patterning PDMS chips were fabricated by soft lithography. The master mold for the PDMS was prepared by either a negative photoresist, SU8 2010 with photolithography or a silicon hard mold with a deep reactive ion etching (DRIE) process. The mold has long meandering channel lines with 20 μm in width and height, respectively. The mixture of Sylgard PDMS (Corning) prepolymer and curing agent in 10:1 ratio (v/v)

was poured onto the mold and cured at 80°C for 1 h. The cured PDMS slab was released from the mold, inlet/outlet holes punched, and bonded onto a poly-L-lysine-(PLL)-coated glass slide (Thermo scientific) to form enclosed channels. The number of microfluidic channels determines the size of the barcode array and 13 parallel microchannels were used in this study.

Once the channels are formed, 13 orthogonal DNA oligomer solutions (sequences are provided in Table 3.1) in a 1:2 mixture (v/v) of 1xPBS buffer and dimethyl sulfoxide (DMSO) were flowed into each of the microfluidic channels. Then the DNA-solution-filled chip was placed in desiccators until the solvent was evaporated completely, leaving the DNA molecules behind. As the last step, the PDMS elastomer was removed from the glass substrate, and the barcode-patterned DNAs were cross-linked to the PLL by thermal treatment at 80 °C for 4 hours. The slide was gently rinsed with deionized water right before use in order to remove salt crystals formed during the solution evaporation step.

4.2.2 Microfluidic chip fabrication for the detection of protein secretion

The PDMS microfluidic chip for the cell experiment was fabricated by two-layer soft lithography[8]. The push-down valve configuration was utilized with a thick control layer bonded together with a thin flow layer. The molds for the control layer and the flow layer were fabricated with SU8 2010 negative photoresist (~ 20 μm thickness) and SPR 220 positive photoresist (~ 18 μm), respectively. The photoresist patterns for the flow layer were rounded via thermal treatment. The thick control layer was molded with a 5:1 mixture of GE RTV 615 PDMS prepolymer part A and part B (w/w) and the flow layer was formed by spin-coating a 20:1 mixture of GE RTV 615 part A and part B (w/w) on the flow layer

mold at 2000 rpm for 60 sec. Both layers were cured at 80°C for 1 h, followed by aligning the control layer to the flow layer, which was still on its silicon mold. Through an additional 60 min of thermal treatment at 80°C, the two layers were bonded. Afterward, the two-layer PDMS chip was peeled off, cut, and access holes punched. As a final step, the two-layer PDMS chip was thermally bonded to the barcode-patterned glass slide, forming the working device.

4.2.3 Cell culture

Human GBM cell lines were cultured in DMEM (American Type Culture Collection, ATCC) supplemented with 10% fetal bovine serum (FBS, Sigma-Aldrich). Human U87MG (U87) GBM cells were purchased from ATCC. The U87EGFR and U87EGFRvIII cell lines were kindly provided by Dr. Paul Mischel (Department of Pathology, University of California at Los Angeles, Los Angeles, CA). For the GBM1600 cell experiments, a low passage primary cell line was established from tumor tissue obtained from a GBM patient. Briefly, the tumor was diagnosed intraoperatively by a board-certified neuropathologist, finely minced with scalpels and resuspended in complete Iscove's modified Dulbecco's medium, supplemented with 20% FBS, 2 mM glutamine, 5 micrograms/ml of insulin and transferrin and 5 ng/ml selenium and a cell line was established in accordance with UCLA-IRB approved human subjects protocol 04-07-020-11.

4.2.4 On-chip secretion profiling

As a first step, the DNA barcode array was transformed into an antibody microarray. The chip was treated with fibronectin (1 μg/mL in phosphate buffered saline (PBS)) by

flow, followed by blocking with 1% bovine serum albumin (BSA) in PBS to prevent non-specific binding. This 1% BSA/PBS solution was used as a working buffer for most of the steps. After blocking, a 200 μl cocktail containing all 12 DNA-antibody conjugates at 30 ng/ml in working buffer was flowed through the micro channels for 1 h. The unbound DNA-antibody conjugates were washed off with 100 μl of fresh buffer. Then, cells were introduced to the microfluidic channels and microfluidic valves were closed by applying 15–20 psi constant pressure to convert 30 microfluidic channels to the 360 isolated microchambers. The chip was incubated in a cell incubator (37°C, 5% CO_2) for 24 h. After the incubation, the chip was removed from the incubator, valves were released, and a 200 μl cocktail containing all biotin-labeled detection antibodies (~ 30 ng/ml) in working buffer was flowed through the microchannels. Next, a 200 μl mixture of 100 ng/ml Cy5-labeled straptavidin and 20 ng/ml Cy3-labeled M' ss DNA in working buffer were flowed through the microchannels, which completed the immune-sandwich assay. Finally, the microchannels were rinsed by flowing working buffer, followed by peeling off the PDMS chip, rinsing the microarray slide with 1×PBS, 0.5×PBS, and deionized water, sequentially, and spin-drying.

4.2.5 Data analysis

The microarray slide was scanned with the GenePix 200B (Axon Instruments) for the fluorescence image of both Cy3 and Cy5 channels. All scans were performed with the same setting of 50% (635 nm) and 15% (532 nm) laser power, 500 (635 nm) and 450 (532 nm) optical gain. Line profiles for the fluorescence intensity of each channel were obtained with the ImageJ software (NIH) and a home-developed Excel macro was employed to

match averaged fluorescence signals for all the barcodes in each chamber to the cell number. The collected data were clustered by Cluster 3.0 and all the heat maps were generated by Java Treeview (http://rana.lbl.gov/EisenSoftware.htm). The bulk secretion data were analyzed by ImageJ.

4.3 Results and Discussion

4.3.1 Multiple-protein secretion profiling from single cells and small cell colonies with integrated microchip

We developed an integrated microfluidic chip to measure proteins from single cells or small cell colonies. The chip is composed of two layers. The lower layer (flow layer) has 30 parallel channels 200 μm in width and 18 μm in height. The top layer (control layer) also has 12 channels perpendicular to the channels in the lower layer which function as valves. When pressure is applied to the channels in the control layer, 360 isolated chambers are formed from the 30 parallel channels. The length of each chamber is 1.8 mm, yielding ~ 6.5 nl of volume per chamber. Owing to this small volume, the secreted protein concentration built up during the incubation time reaches a high enough level to be quantitatively measured even from a single cell.

We utilized a miniaturized antibody barcode array based on the DNA-encoded antibody library (DEAL) approach[9] to detect secreted proteins. First, DNA barcode array in the form of parallel stripes with 20 μm and 40 μm in width and pitch, respectively, is generated based on the microchannel-guided flow patterning technology. The DNA barcode array is transformed to the antibody barcode array by hybridizing DEAL conjugates (antibodies

conjugated to the complementary DNAs)[10]. The array for this study is designed for 13 stripes: 12 stripes for proteins and 1 stripe for an alignment reference.

Cells are randomly loaded into the large array of microchambers, which results in one or a small number of cells per chamber. The loaded cells can be imaged owing to the transparency of the chip. The schematics of the chip platform and the protein detection scheme are illustrated in Figs. 4.1a and 4.1b, respectively. The 12 proteins used for this study are as follows: interleukin (IL)-2, monocyte chemotactic protein (MCP)-1, IL-6, granulocyte-colony stimulating factor (G-CSF), macrophage inhibitory factor (MIF), epidermal growth factor (EGF), vascular endothelial growth factor (VEGF), platelet-derived growth factor (PDGF-AB), transforming growth factor (TGF)-α, IL-8, IL-1ra, and hepatocyte growth factor (HGF). For some experiments EGF and PDGF-AB are replaced with matrix metallo-proteases (MMP) 3 and IL-1β. Fig. 4.1c shows representative microchambers loaded with four, three, and two U87 cells, along with the scanned images. The device presents a good signal-to-noise ratio for the detection of multiple secreted proteins.

4.3.2 Secretion profile from integrated barcode chip vs. bulk experiment

Our integrated barcode chip platform allows high-content analysis on many cell secretion events per chip. Fig. 4.2a shows three heat maps generated from on-chip experiments with U87, U87EGFR, and U87EGFRvIII GBM cell lines, respectively. Signals from single cells to ~ 20 cells were obtained and the secretion of 6 proteins was clearly identified from all cell lines. There are slightly different trends in terms of secretion profile among the three cell lines, even though they are from the same lineage. The major

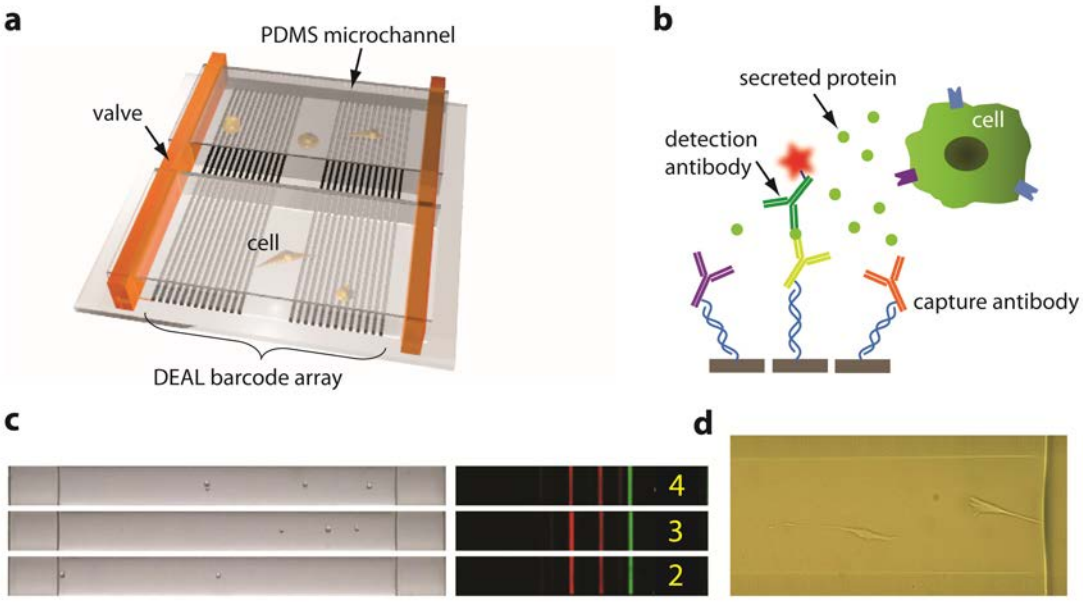

Figure 4.1 Integrated barcode chip for secreted protein profiling from single cells and small cell colonies. (a) Schematic drawing of the major components of the device. Each microchamber has two repeats of 13 barcode patterns for antibody array converted from DNA array. (b) The mechanism of detection for the secreted proteins from cells. Secreted proteins are captured by capture antibodies patterned on the substrate and visualized by a sandwich assay with biotin-labeled detection antibodies and cy5-labeled streptavidin. (c) Representative microchambers with four, three, and two cells, along with scanned fluorescence images of barcode signals. Red bars represent protein signal and green bars represent signals for the position reference. (d) Optical image of cells in the device after 24 h of incubation. Fibronectin coating allows cells to stay alive in a healthy condition. Cells even move, grow, and divide in the chamber during incubation.

difference among the three cell lines is the epidermal growth factor receptor (EGFR) activity; U87EGFR cells have amplified EGFRs and U87EGFRvIII cells have ligand-independent, constitutively activated EGFR. Thus, different secretion profiles may reflect the effect of EGFR activity on these cells. The bulk secretion measurements for U87 and U87EGFRvIII cells were also performed with a conventional microarray. Similar profiles of secreted proteins to the on-chip experiments were obtained (Fig. 4.2c). However, it was difficult to resolve the difference between two cell types. In order to quantitatively compare

the differences, letter maps based on the signal intensities were generated in Fig. 4.2b and 4.2d. The relative signal intensities of each protein to the reference signal were calculated and the values were used as a font size. In Fig. 4.2d, U87 and U87EGFRvIII from the bulk experiments show almost identical letter maps. In contrast, letter maps of three cell lines from on-chip experiments show differences in terms of signal intensities for major proteins secreted. Most proteins including IL-6, MIF, VEGF, and IL-8 tend to be secreted more as the EGFR activity is stronger. HGF signal was weaker for U87EGFRvIII cells than others. This letter map analysis reveals that we can get more information from the on-chip experiment, information that is difficult to resolve from the conventional bulk experiment. The information from single cells or small colonies of cells, when combined together with the bulk experimental results, can lead us to understand the biology of cells more clearly.

4.3.3 Single-cell protein secretion profiling of GBM cell line: U87 cells

For comparison, the data from a single cell, three cells, and many cells (more than 6 cells) were extracted and analyzed with an unsupervised clustering by Cluster 3.0 software (Fig. 4.3a). Each row in the heat map represents the data from a single chamber. Here 70 single cell data sets were collected and several notable features can be extracted from this analysis. The most striking observation is the anti-correlation between MIF and VEGF / IL-8. This anti-correlation can be found from the single-cell data and the effect becomes weaker as the cell number increases (Fig. 4.3a). It is difficult to identify this relationship from even three-cell data. To quantitatively analyze this, we plotted the scattered plots for single cell and three cells which show the correlation among MIF, VEGF, and IL-

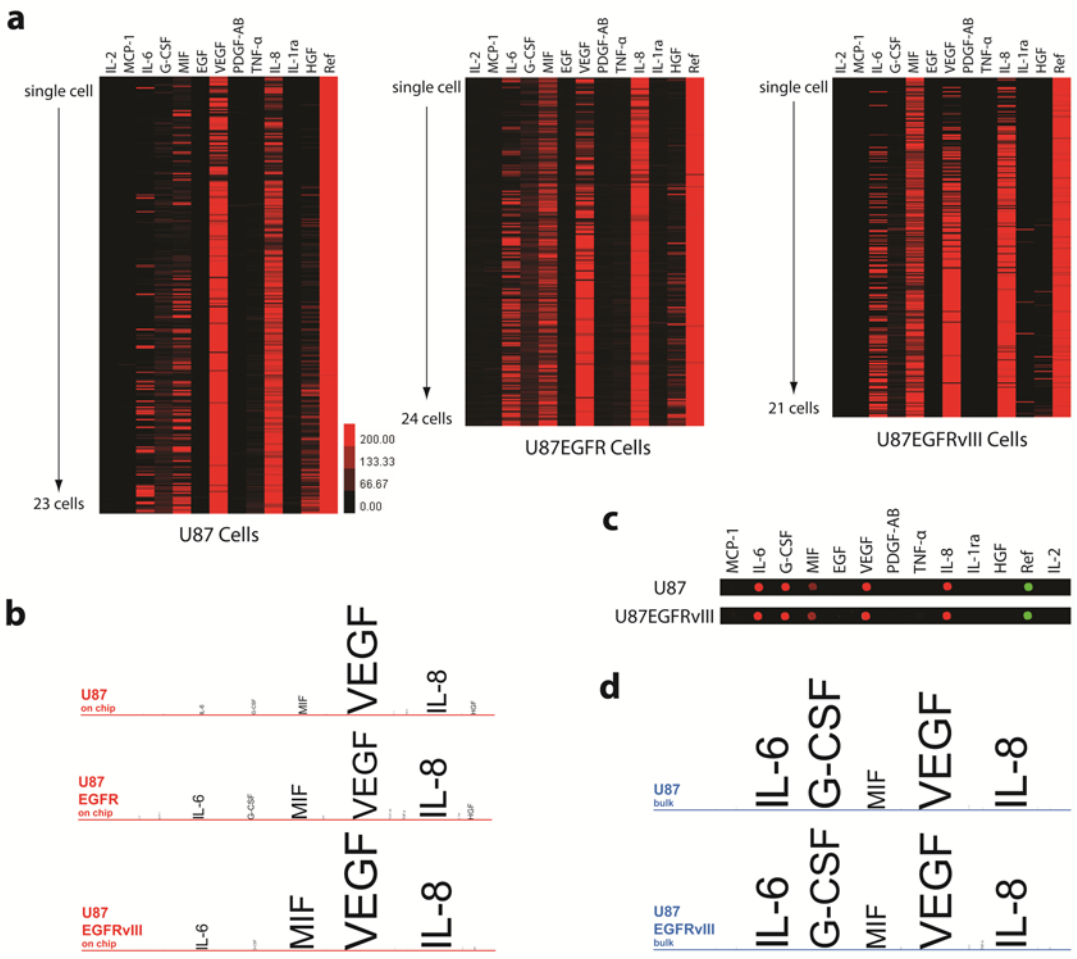

Figure 4.2 Secretion profiles from GBM cell lines: integrated barcode chip vs. bulk experiment. (a) Heat maps showing the fluorescence intensities of barcodes corresponding to the measurement of 12 proteins as the cell number increases from one to ~ 20 for U87, U87EGFR, and U87EGFRvIII cells. (b) Letter maps generated based on the relative fluorescence intensities of proteins to the reference signal intensity from the on-chip experimental data. The font size represents the relative signal intensity. (c) Scanned images showing the secretion profiles of U87 and U87EGFRvIII cells cultured in a petri dish for 24 h. Conventional pit-spotted DNA microarray along with DEAL technique was used for the bulk measurement. (d) Letter maps generated from bulk experimental data

8. The data from the chambers with zero cells were used as a gate for the background reference (black rectangles) and the data from the single cell or three cells were plotted with red circles in Figs. 4.3b and 4.3c. The circles in each quadrant were counted and

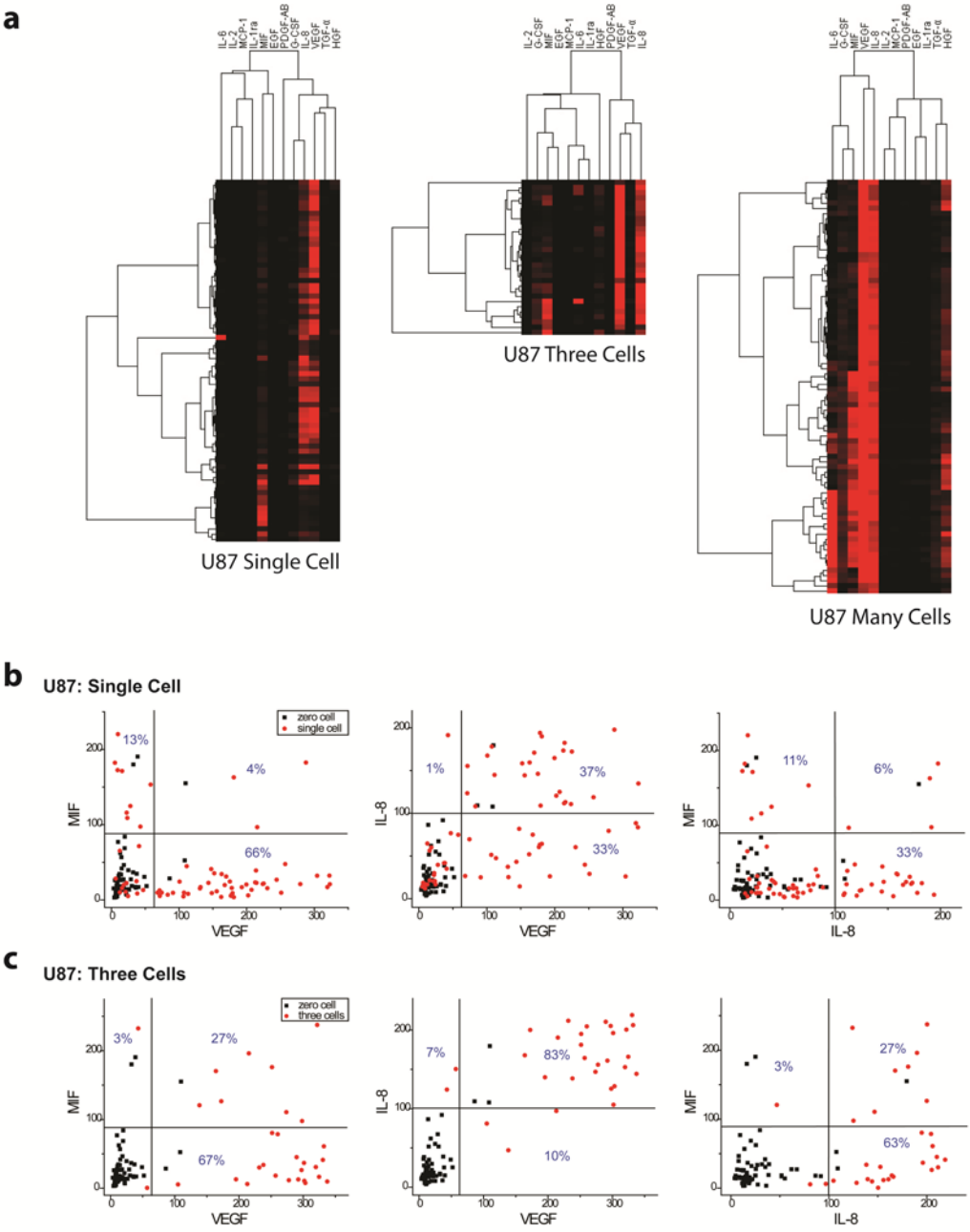

Figure 4.3 Single-cell secretion profiles for U87 cells. (a) Heat maps from clustered data sets of single cells, three cells, and many cells (more than 6). Data for specific number of cells are collected and clustered with an unsupervised method. (b) Scatter plots of MIF, VEGF, and IL-8 for single cells. (c) Scatter plots of MIF, VEGF, and IL-8 for three cells.

represented to quantitatively identify the relationships between two proteins. We found 13% $MIF^{+}|VEGF^{-}$ and 66% $MIF^{-}|VEGF^{+}$ events from the single cell and only 4% of single-cell events showed $MIF^{+}|VEGF^{+}$, which confirms the anti-correlations between MIF and VEGF. Interestingly, from three-cell data, only 3% $MIF^{+}|VEGF^{-}$ events were found and 27% of the events showed $MIF^{+}|VEGF^{+}$. Thus, we can identify the transition from the anti-correlation to the positive correlation as the cell number increases. This is an interesting observation because it was reported that there is a positive correlation between MIF and VEGF expression with a bulk scale analysis in GBM[11] and we also noticed a similar trend in the bulk analysis. The unique feature of an anti-correlation at the single-cell level can offer us another opportunity to find out unknown pathways related to the two potent angiogenic factors in GBM, VEGF and MIF.[11, 12] IL-8 shows positive correlation with VEGF and thus anti-correlation with MIF.

Another interesting feature can be found from the columns of the heat map. For the clustering, we also included the correlations among proteins, which clusters the proteins as well. In the single-cell heat map, there are two major clusters, one with MIF and the other with VEGF and IL-8, and this can represent the anti-correlation among them again. However, in the heat map for many cells, they are in the same cluster, which represents the transition from the anti-correlation to the positive correlation. IL-6 can also be found in the heat map for many cells and this may reflect a possible paracrine signal for IL-6 secretion, which will be discussed below.

4.3.4 Cell–cell communication effect

Owing to the transparency of PDMS, we can monitor the experimental process optically and this feature also enables us to connect physical properties of cells or microenvironment to the cell physiology. Many different factors such as oxygen level[13], cell morphology including size and shape,[14] temperature,[15] and cell–cell interaction[16] are correlated to cell behavior. Therefore it is useful to be able to monitor the cell morphology or the environment and to match them with the protein-secretion profiles. As an example, we measured the distance between two cells and analyzed the protein-secretion profiles based on the information. In Fig. 4.4a, representative data sets from the U87EGFR experiment for the chambers with two cells and three cells are presented. Cells secrete more proteins as they are located closer. It can be easily seen that IL-6 and VEGF signals are stronger for the chambers with closely located cells. To analyze this effect quantitatively, scatter plots for protein-secretion level and cell–cell distance were generated based on 34 data sets and 52 data sets from U87 and U87EGFR cells, respectively (Figs. 4.4b and 4.4c). U87EGFR cells show stronger secretion levels for IL-6 and VEGF when cells are closely located, which represents a possible paracrine effect for the secretion of these two proteins. Interestingly, the cell–cell communication effect is not seen in the case of U87 cells. Based on this observation, we can conclude that there exists a paracrine signaling for IL-6 and VEGF secretion and it is related to the EGFR activity. This cell–cell communication effect presents another useful application of this device to study tumor microenvironment systemically. Even though we used the cell–cell distance as a representative parameter in this study, we can also monitor the cell morphology,

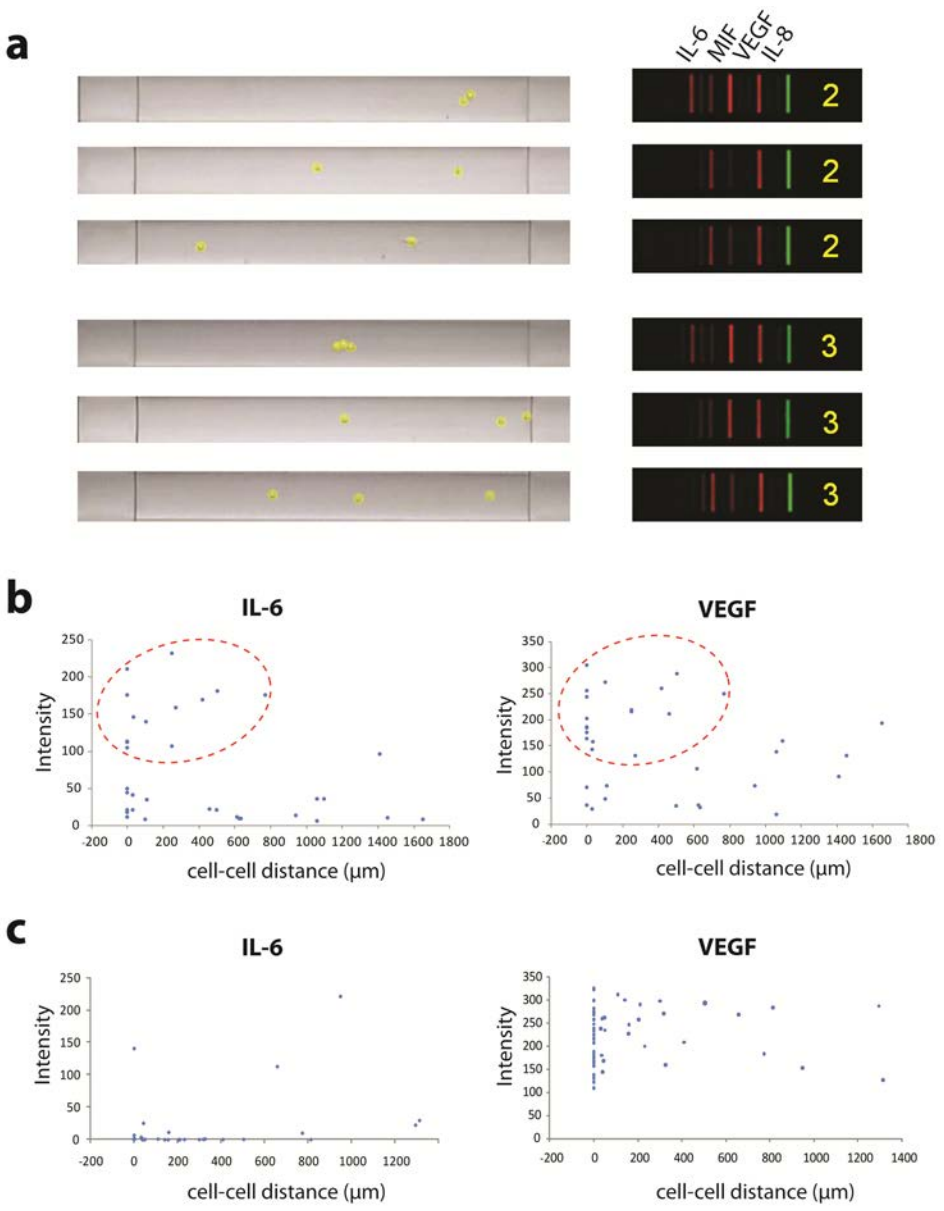

Figure 4.4 Distance effect for cell–cell communication. (a) Representative optical images for U87EGFR cells in microchambers along with the secretion profile. Closely located cells show high level of secretion especially for VEGF and IL-6. (b) Scatter plots of signal intensity vs. cell–cell distance for U87EGFR cells. (c) Scatter plots of signal intensity vs. cell–cell distance for U87 cells

proliferation rate, motility, and size, etc., with the current design or a slightly modified design.

4.3.5 PTEN activity on GBM cell line: U87EGFRvIII vs. U87EGFRvIII/PTEN

Studying major pathways related to cancer is useful in understanding basic cancer biology as well as in finding new treatment of the disease. Many drugs are inhibitors of specific proteins that play important roles to maintain unique features of cancer such as angiogenesis, immortality, and metastasis. Therefore monitoring secreted proteins, combined with the knowledge of the related signaling pathways, can offer another way of understanding cancer and finding treatment. We further interrogate PTEN, a protein

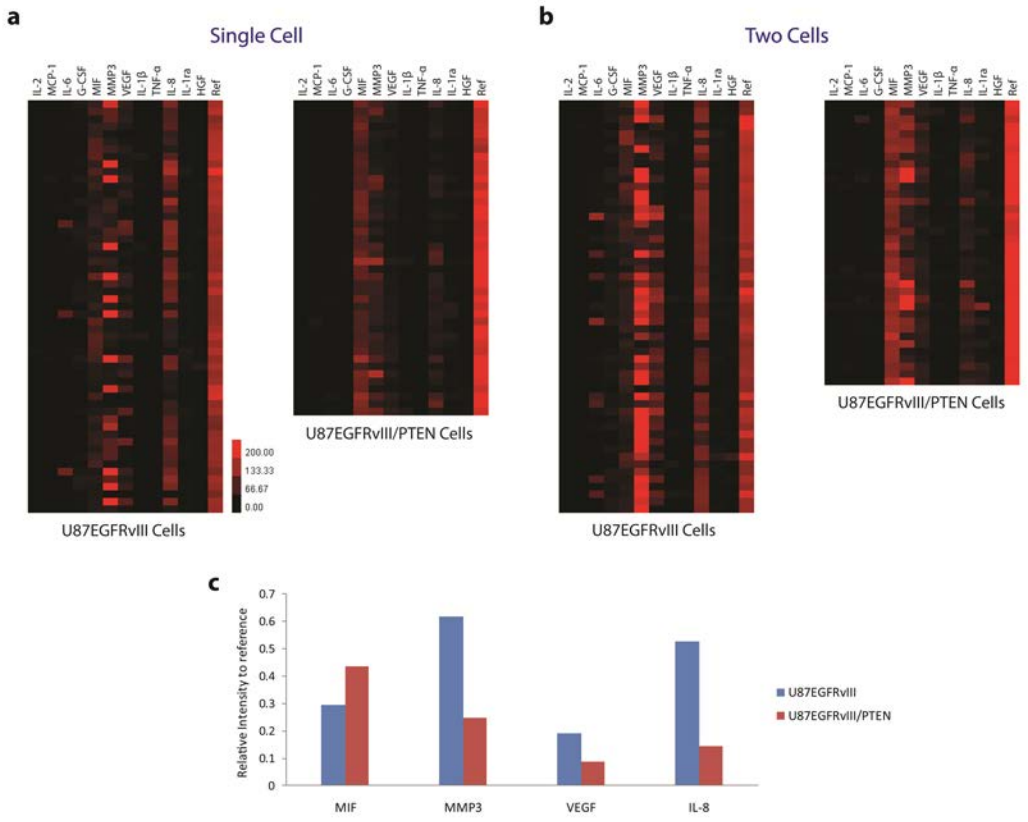

Figure 4.5 PTEN activity in U87EGFRvIII cells revealed by protein secretion profiling. (a) Heat maps derived from single-cell secretion data of U87EGFRvIII and U87EGFRvIII/PTEN cells. (b) Heat maps derived from two-cell secretion data of U87EGFRvIII and U87EGFRvIII/PTEN cells. (c) Relative intensities of MIF, MMP3, VEGF, and IL-8 signals to the reference signal for U87EGFRvIII and U87EGFRvIII/PTEN cells

encoded by a tumor-suppressor gene, *PTEN*, and its effect on U87EGFRvIII cells as an example. PTEN is known to negatively regulate intracellular levels of phosphatidylinositol-3,4,5-triphosphate which is in upstream of Akt/PKB signaling pathway. Also in GBM cells, it was reported that PTEN mutation can cooperate with EGFR activation to increase VEGF mRNA levels via PI3K/AKT pathway.[17] U87 cells have a PTEN mutation[17] and so do U87EGFRvIII cells, because they have been derived by retroviral transduction of U87 cells with pLPCX constructs that contain EGFRvIII cDNA.[18] Thus, U87EGFRvIII cells have a sufficient condition for the up-regulation of VEGF, which can be identified from Figs. 4.5a and 4.5b. Figs. 4.5a and 4.5b show heat maps for secreted proteins from U87EGFRvIII and U87EGFRvIII/PTEN, respectively, at the single-cell and two-cell level. Here the protein panel is slightly modified by replacing EGF and PDGF-AB with MMP3 and IL-1β, respectively. U87EGFRvIII/PTEN cells show very weak VEGF signal, as expected. In Fig. 4.5c, the relative signal intensities to the reference signal for the four major proteins, including VEGF, are plotted. It can be easily seen that VEGF, MMP3, and IL-8 are positively correlated and U87EGFRvIII/PTEN cells show a much lower signal intensity of them. On the other hand, the MIF signal is stronger for U87EGFRvIII/PTEN cells, and this observation is supported by the anti-correlation between MIF and VEGF found in Figs. 4.3a and 4.3b. The results obtained from U87EGFRvIII and U87EGFRvIII/PTEN reveal the tumor suppressing effect of PTEN by down-regulating pro-angiogenic factors, including VEGF, MMP3, and IL-8, which might be related to the PI3K/Akt pathway.

4.3.6 Toward clinical sample: analysis on GBM primary tumor cells

To demonstrate the utility of our device for analyzing clinical specimens and for probing the molecular heterogeneity of pathogenesis, we performed an on-chip secretion profiling of solid tumor cells at the single-cell level. A low-passage primary GBM culture (GBM 1600 cells) was established from a surgically resected GBM tumor.[19] (The tumor was diagnosed intraoperatively by a board-certified neuropathologist.) Tumor-secreted

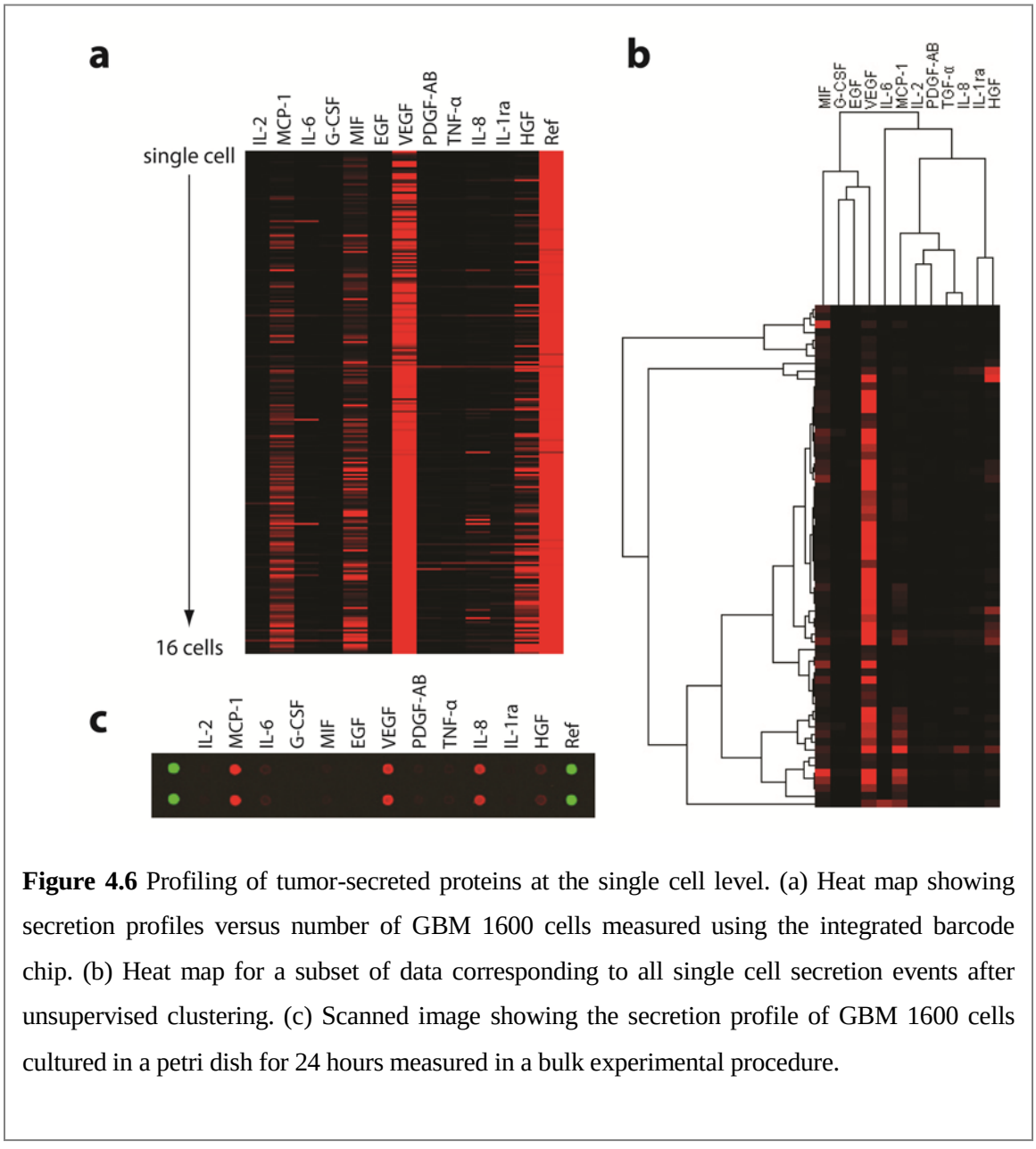

Figure 4.6 Profiling of tumor-secreted proteins at the single cell level. (a) Heat map showing secretion profiles versus number of GBM 1600 cells measured using the integrated barcode chip. (b) Heat map for a subset of data corresponding to all single cell secretion events after unsupervised clustering. (c) Scanned image showing the secretion profile of GBM 1600 cells cultured in a petri dish for 24 hours measured in a bulk experimental procedure.

soluble factors play a critical role in shaping the tumor microenvironment and inducing metastasis.[20] Thus, analysis of protein-secretion profiles at the single-cell level from small amounts of clinical specimens, e.g., tumor tissues, has important implication in cancer diagnosis and sub-typing.

Results from a single microchip (Fig. 4.6a) revealed the secretion of at least six proteins (MCP-1, IL-6, MIF, VEGF, IL-8, and HGF), while the negative control, IL-2, did not show any appreciable signal. We further analyzed the single-cell secretion events with clustering (Fig. 4.6b). It is interesting that the major secreted proteins are very similar to those from U87 cell lines. The GBM 1600 cells displayed highly heterogeneous activities, which can provide insight into the heterotypic nature of tumor cells, as we also noticed from the cell line. This experiment demonstrated the utility of this approach for the multifunctional profiling of cells harvested from clinical specimens such as tumor tissues.

4.4 Conclusions

Traditional assays for cellular functions provide averaged information from a large population of cells. This information alone, however, cannot represent the real biology of a complex, heterogeneous system such as a tumor. Most of time we can miss the hidden players or pathways that are critical to understanding the phenomena. The anti-correlation between MIF and VEGF that we observed with our integrated barcode chip is a good example of that. Previous reports based on a conventional approach showed only a positive correlation. We further identified the transition from the anti-correlation to the positive correlation as the cell number increases. More in-depth study is required to find the mechanism for the anti-correlation. This observation, however, still reflects that there might

be some facts that we are missing by making conclusions solely based on the conventional, bulk experimental data. We noticed highly heterogeneous functions even from the same lineage of cells at the single-cell level. This might be just an intrinsic complexity of biological processes such as cell–cell interaction and stochastic gene expression. But it is also true that the heterogeneity plays important roles in human health, whose outcome is the collective phenomena that we can observe with the bulk analysis. By analyzing heterogeneous but large amounts of data from single cells or small cell colonies, we can add an additional technique that can change our way of looking at diseases or basic biology. Our integrated barcode chip platform can help to disentangle at least some aspects of heterogeneous cellular responses.

Complexity is the major bottleneck for attacking cancer. That is why we need to use a tool for multi-parameter analysis and an approach to systemically study the collected information.[2] However, the single-parameter assay is still used in clinics because of the lack of a simple and inexpensive multi-parameter analysis tool. The recent failure of an HIV vaccine clinical trial by Merck can be a good example of the importance of a multi-parameter-based approach. Furthermore, the examination of cellular functions in a heterogeneous lesion is critical for the accurate diagnosis of complex human diseases such as cancer.[21] Our integrated barcode chip platform offers a functionality of multi-parameter analysis not only from the secreted protein profiling but also from the combined analysis of physical characteristics of cells and the environment. Through the cell–cell interaction study, we confirmed that VEGF and IL-6 are secreted in a paracrine manner through EGFR. This is a simple example of what we can find out by adding information from a different angle. By utilizing small chambers with status that we can easily track during the

experiment, we can study the effect of physical, environmental factors such as temperature, geometry, oxygen level, and drugs on cells. Ease of fabrication is a major advantage of a PDMS-based platform, as is the optical transparency. Therefore we can easily modify the design and expand the scope of what we can study, especially for the tumor microenvironment.

From the experiments with U87 cell lines, we noticed the heterogeneity of cell behavior at the single-cell level, which might present clues for understanding deep biology. Through perturbation tests, such as neutralization of specific cytokines or growth factors and drug treatment, we can study the network of signaling pathways and apply the findings to disease diagnostics or treatment. Studying cell lines with a different set of mutations or characteristics enables us to build up an informative database as well. As an example, we confirmed PI3K/Akt-dependent PTEN activity by testing U87EGFRvIII cells and U87EGFRvIII/PTEN cells with our platform. If we collect data sets from many different cell lines for a specific cancer, it can provide a good reference for systemic analysis towards personalized diagnostics and treatments. We also applied the integrated barcode chip platform to perform multiplexed secreted-protein profiling of primary tumor cells. The response was also heterogeneous and complex. However, by combining these results with conventional diagnostic tests, we can use our platform for clinical applications, especially when we have a library of data sets for specific mutations related to cancer. Kotecha et al. showed the existence of unique cellular signatures of tumors that are useful for patient stratification with flow cytometry as well.[22] Recently Kwong et al. reported cell sorting with DEAL and Nucleic Acid Cell Sorting (NACS) technologies.[23] If we combine these technologies with our platform, we can sort specific cell types from a cancer patient's

tissue sample and characterize them based on protein-secretion profiling. The integrated barcode chip represents a highly multiplexed, sensitive, and inexpensive platform that offers potential use in assessing functional heterogeneity of cells in complex disease lesions by examining clinical samples (e.g., skinny-needle-biopsied tissue). It also has the potential to analyze a disease-associated signaling network from individual patients for use in differential diagnosis and personalized treatment.

4.5 References

1. Heath, J. R.; Davis, M. E., Nanotechnology and cancer. *Annual Review of Medicine* **2008**, 59, 251–265.
2. Heath, J. R.; Phelps, M. E.; Hood, L., NanoSystems biology. *Molecular Imaging and Biology* **2003**, 5, (5), 312–325.
3. Khalil, I. G.; Hill, C., Systems biology for cancer. *Current Opinion in Oncology* **2005**, 17, (1), 44–48.
4. Mueller, M. M.; Fusenig, N. E., Friends or foes - bipolar effects of the tumour stroma in cancer. *Nature Reviews Cancer* **2004**, 4, (11), 839–849.
5. Sachs, K.; Perez, O.; Pe'er, D.; Lauffenburger, D. A.; Nolan, G. P., Causal protein-signaling networks derived from multiparameter single-cell data. *Science* **2005**, 308, (5721), 523–529.
6. Cox, J. H.; Ferrari, G.; Janetzki, S., Measurement of cytokine release at the single cell level using the ELISPOT assay. *Methods* **2006**, 38, (4), 274–282.

7. Liang, Y.; Diehn, M.; Watson, N.; Bollen, A. W.; Aldape, K. D.; Nicholas, M. K.; Lamborn, K. R.; Berger, M. S.; Botstein, D.; Brown, P. O.; Israel, M. A., Gene expression profiling reveals molecularly and clinically distinct subtypes of glioblastoma multiforme. *Proceedings of the National Academy of Sciences of the United States of America* **2005**, 102, (16), 5814–5819.
8. Thorsen, T.; Maerkl, S. J.; Quake, S. R., Microfluidic large-scale integration. *Science* **2002**, 298, (5593), 580–584.
9. Bailey, R. C.; Kwong, G. A.; Radu, C. G.; Witte, O. N.; Heath, J. R., DNA-encoded antibody libraries: a unified platform for multiplexed cell sorting and detection of genes and proteins. *Journal of the American Chemical Society* **2007**, 129, (7), 1959–1967.
10. Fan, R.; Vermesh, O.; Srivastava, A.; Yen, B. K.; Qin, L.; Ahmad, H.; Kwong, G. A.; Liu, C. C.; Gould, J.; Hood, L.; Heath, J. R., Integrated barcode chips for rapid, multiplexed analysis of proteins in microliter quantities of blood. *Nature Biotechnology* **2008**, 26, (12), 1373–1378.
11. Munaut, C.; Boniver, J.; Foidart, J. M.; Deprez, M., Macrophage migration inhibitory factor (MIF) expression in human glioblastomas correlates with vascular endothelial growth factor (VEGF) expression. *Neuropathology and Applied Neurobiology* **2002**, 28, (6), 452–460.
12. Bacher, M.; Schrader, J.; Thompson, N.; Kuschela, K.; Gemsa, D.; Waeber, G.; Schlegel, J., Up-regulation of macrophage migration inhibitory factor gene and protein expression in glial tumor cells during hypoxic and hypoglycemic stress indicates a critical role for angiogenesis in glioblastoma multiforme. *American Journal of Pathology* **2003**, 162, (1), 11–17.

13. Brown, J. M.; Wilson, W. R., Exploiting tumour hypoxia in cancer treatment. *Nature Reviews Cancer* **2004**, 4, (6), 437–447.

14. Behnam-Motlagh, P.; Grankvist, K.; Henriksson, R.; Engstrom, K. G., Response in shape and size of individual p31 cancer cells to cisplatin and ouabain: a computerized image analysis of cell halo characteristics during continuous perfusion. *Cytometry* **2000**, 40, (3), 198–208.

15. Levine, E. M.; Robbins, E. B., Differential temperature sensitivity of normal and cancer cells in culture. *Journal of Cellular Physiology* **1970**, 76, (3), 373–379.

16. Goswami, S.; Sahai, E.; Wyckoff, J. B.; Cammer, M.; Cox, D.; Pixley, F. J.; Stanley, E. R.; Segall, J. E.; Condeelis, J. S., Macrophages promote the invasion of breast carcinoma cells via a colony-stimulating factor-1/epidermal growth factor paracrine loop. *Cancer Research* **2005**, 65, (12), 5278–5283.

17. Pore, N.; Liu, S.; Haas-Kogan, D. A.; O'Rourke, D. M.; Maity, A., PTEN mutation and epidermal growth factor receptor activation regulate vascular endothelial growth factor (VEGF) mRNA expression in human glioblastoma cells by transactivating the proximal VEGF promoter. *Cancer Res*earch **2003**, 63, (1), 236–241.

18. Wang, M. Y.; Lu, K. V.; Zhu, S.; Dia, E. Q.; Vivanco, I.; Shackleford, G. M.; Cavenee, W. K.; Mellinghoff, I. K.; Cloughesy, T. F.; Sawyers, C. L.; Mischel, P. S., Mammalian target of rapamycin inhibition promotes response to epidermal growth factor receptor kinase inhibitors in PTEN-deficient and PTEN-intact glioblastoma cells. *Cancer Res*earch **2006**, 66, (16), 7864–7869.

19. Wang, Y.; Zhu, S.; Cloughesy, T. F.; Liau, L. M.; Mischel, P. S., p53 disruption profoundly alters the response of human glioblastoma cells to DNA topoisomerase I inhibition. *Oncogene* **2004**, 23, (6), 1283–1290.

20. Kim, S.; Takahashi, H.; Lin, W. W.; Descargues, P.; Grivennikov, S.; Kim, Y.; Luo, J. L.; Karin, M., Carcinoma-produced factors activate myeloid cells through TLR2 to stimulate metastasis. *Nature* **2009**, 457, (7225), 102–106.

21. Visvader, J. E.; Lindeman, G. J., Cancer stem cells in solid tumours: accumulating evidence and unresolved questions. *Nature Reviews Cancer* **2008**, 8, (10), 755–768.

22. Kotecha, N.; Flores, N. J.; Irish, J. M.; Simonds, E. F.; Sakai, D. S.; Archambeault, S.; Diaz-Flores, E.; Coram, M.; Shannon, K. M.; Nolan, G. P.; Loh, M. L., Single-cell profiling identifies aberrant STAT5 activation in myeloid malignancies with specific clinical and biologic correlates. *Cancer Cell* **2008**, 14, (4), 335–343.

23. Kwong, G. A.; Radu, C. G.; Hwang, K.; Shu, C. J.; Ma, C.; Koya, R. C.; Comin-Anduix, B.; Hadrup, S. R.; Bailey, R. C.; Witte, O. N.; Schumacher, T. N.; Ribas, A.; Heath, J. R., Modular nucleic acid assembled p/MHC microarrays for multiplexed sorting of antigen-specific T cells. *Journal of the American Chemical Society* **2009**, 131, (28), 9695–9703.